Experimental Mechanics (2016) 56:683–701
DOI 10.1007/s11340-015-0120-3

Residual Stress Analysis of Ceramic Coating by Laser Ablation and Digital Holography

G. Pedrini[1] · V. Martínez-García[2] · P. Weidmann[3] · M. Wenzelburger[2] · A. Killinger[2] · U. Weber[3] · S. Schmauder[3] · R. Gadow[2] · W. Osten[1]

Received: 7 May 2015 / Accepted: 16 December 2015

Abstract In this paper, a method for residual stress analysis of ceramic coatings by applying a laser for quasi non-destructive material removal and measuring the 3D displacement around the machined area by means of high-resolution digital holography is described. The residual stresses are retrieved by numerical calculations using the finite element method (FEM) from the measured 3D displacements, the profile of the machined hole and the material parameters of the coating and substrate. Experimental results on thermal spray coatings together with discussion of the difficulties, work in progress, potential of the method, and comparative measurements by the hole-drilling method are presented.

Keywords Residual stress · Layer composites · Hole-drilling method · Thermal spraying · Pulsed laser · Digital holography · Finite element method

Introduction

Ceramic coatings are commonly used to improve the wear or heat resistance of many technical components or to provide electrically non-conductive surfaces. But due to their application process, e.g. plasma or high-velocity oxy-fuel spraying, rather high residual stresses can be generated within the coating and underneath. The main reasons for that are differences in the coatings and substrates expansion coefficients, inhomogeneously distributed temperatures during the process and the quenching of splats [1].

For the analysis of residual stresses in layer composites or in coatings, a variety of techniques can be used. The diffraction methods apply X-ray, synchrotron or neutron radiation for the measurement of the Bragg angle which is influenced by crystal lattice deformations due to residual stresses. The measured lattice deformations are used for the calculation of the residual stresses of first, second and third order (sub-microscopic stresses on the atomic scale) [1, 2]. These methods are time consuming, and thus not suitable to be used inline during the coating process. Methods based on eddy currents, Barkhausen noise or induction can be used for residual stress measurements on conductive or magnetic samples [3], but unfortunately, can usually not be applied to ceramic coating composites.

The hole drilling technique is a quasi-non-destructive method with the advantage of time/cost efficient application and the possibility of in-situ measurements, without neglecting a good depth resolution and quantitative accuracy [4–7]. The residual stresses in the layer composite are locally released due to the material removal, which leads to a displacement of the surface around the hole. These displacements, usually measured as relaxed strains by strain gauge rosettes, in combination with appropriate calibration data (separately determined by simulation for the layer composite), allows the quantitative determination of the residual stress/depth profiles. The disadvantage of the strain gauges is that they can only be used on flat and relatively smooth surfaces, where the rosette is applied. Furthermore, they measure only in-plane strains (2-dimensional). Since the distance between

---

✉ G. Pedrini
pedrini@ito.uni-stuttgart.de

[1] Institut für Technische Optik (ITO), University of Stuttgart, Stuttgart, Germany

[2] Institut für Fertigungstechnologie keramischer Bauteile (IFKB), University of Stuttgart, Stuttgart, Germany

[3] Institut für Materialprüfung, Werkstoffkunde und Festigkeitslehre (IMWF), University of Stuttgart, Stuttgart, Germany

the hole-centre and the strain gauge is always relatively large, there are limitations both in terms of spatial resolution and practicability. The accuracy of the measurements depends as well on the asymmetries of the hole as on the positioning of the strain gauge rosette [1].

Optical approaches based on Electronic Speckle Interferometry (ESPI) can be as well used for the determination of the strains produced by hole drilling [8–14]. Compared with the strain gauges, these optical techniques have the advantage of being contactless, and furthermore, they allow the instant full field measurement of the strain field. Displacements and relative strains can also be measured by digital holographic interferometry [15, 16], which represents a further development of the ESPI technique, where the holograms may be recorded in one shot without using time consuming phase shift procedures. From the digital holograms recorded by illuminating the object from different directions, the 3D displacement of the object with accuracy of some nanometres can be determined. Digital image correlation is another optical technique that is usually used for the measurement of 2D and 3D displacements. Images acquired before and after displacements are analysed by correlating array subsets on two or more corresponding images for extracting the displacements [17]. This non-interferometric technique is much less affected by vibrations compared with ESPI or digital holography, its resolution with 1.3 megapixel cameras can be 1/30,000 of the field of view [18]; this means that displacements of 10 nm can be measured, but in this case, the field of view will be only 300 μm (this can be increased by using cameras with more pixels). In Ref. [19], it is shown how digital image correlation combined with the hole drilling method can be used for the detection of residual stresses.

For the hole drilling, high speed mechanical devices are usually used and a contact between equipment and work piece is unavoidable. Pulsed lasers can be used for machining (e.g. drilling, milling, cutting, soldering, marking), and different technologies (percussion, trepanning, helical drilling) for drilling and milling various materials combined with different lasers (e.g. Nd:YAG laser with nanosecond pulse length, CO_2 laser) are described in the literature [20–22]. Therefore, it seems to be straightforward especially for the investigation of layer composites with a high hardness and wear resistance, as described here, to use a pulsed laser instead of mechanical drilling, to remove precisely material from the object surface.

In this paper, we propose an approach to avoid the mechanical drilling operation and the application of strain gauges, where a pulsed laser is used for the object machining (ablation process) leading to 3D residual displacements by stress relaxation which are measured by an optical system based on digital holographic interferometry. Through the combination of pulsed lasers and spatial light modulators (SLM), adaptive minimally invasive hole geometries (not only circular holes) are produced allowing the controlled release and measurement of the spatially resolved residual stresses. Compared with the existing techniques it has the advantage of being contactless and thus has the capability for the in-situ and in-line measurements during the coating process allowing a controlled deposition of layers with the wanted residual stresses.

In "Residual stresses in thermal spray coatings" Section, we show how residual stresses are produced during the spray coating process and in "Experimental setup and measuring procedure" Section, the laser ablation and 3D displacements measuring system are described. The optically measured surface displacements are used for residual stress calculation by FEM, following a similar procedure as the calculation of calibration factors for conventional hole drilling residual stress analysis. However, the present analysis accounts for 3D surface deformations and the true shape of the laser ablation hole as well as the material parameters of the coating and substrate (see Residual stress evaluation procedure Section). Test objects coated by atmospheric plasma spraying (APS) have been prepared (see Test objects and loading device Section) and used for the experimental verification of the proposed method (see Experimental results Section). The potential and difficulties of the technique are discussed in "Conclusions" section.

Residual Stresses in Thermal Spray Coatings

Thermal spraying techniques are coating processes in which a feedstock inside or outside a spray gun is heated and molten (in fully liquid, semi-molten or partially solid particle state), atomised and propelled towards a substrate, where it is deposited to form a surface coating while the substrate to be coated is not molten [23]. Thus, the coating build-up is due to thermal and kinetic energy of the spray particles, which are flattened during deposition to form so-called splats that adhere to the substrate and one-another by means of mechanical clamping (whereby residual stresses play an important role), physical and chemical adsorptive forces, and cohesion.

Thermal spray processes allow the deposition of a broad variety of coating materials (metals, alloys, ceramics, polymers, and composites) in the form of rods, wire, powder or suspension on a variety of substrates, including light metals, polymers, and even paper. Energy sources can also be manifold, e.g., autogenous flame in high-velocity oxy-fuel (HVOF) spraying or electric arc discharge to form a plasma in atmospheric plasma spraying (APS), which was used for coating application in this work. A general process scheme is given in Fig. 1.

Coating particle temperatures depend on the energy source of the process and can even exceed the melting point of the respective coating material. E.g., the plasma temperature in APS is in the region of 20,000 K. Nevertheless, substrate temperatures remain in the region of below 150–200 °C due to different in-process cooling mechanisms (forced

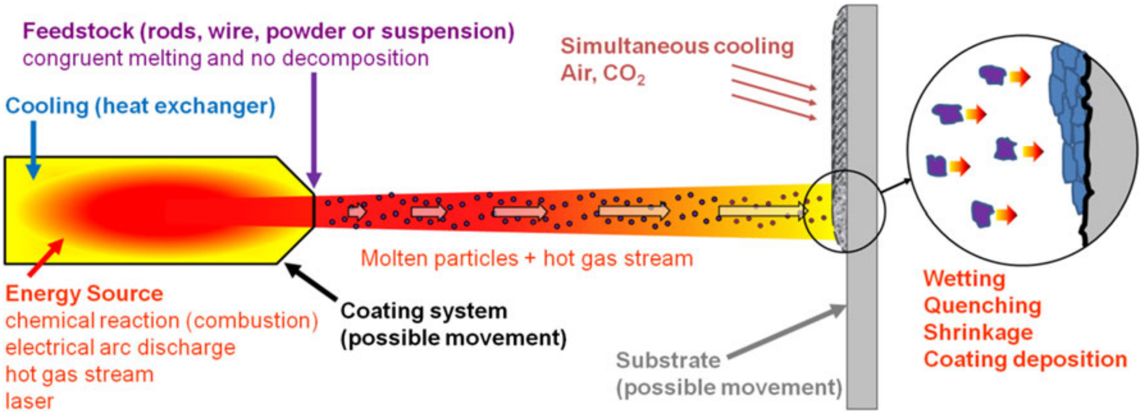

Fig. 1 Thermal spray schematic with energy sources and thermal factors of influence

convection by compressed air or CO_2, natural convection, radiation) and the low deposition rate of material with single particles having the size of 20–50 μm. Solidification occurs rapidly within 10^{-5}–10^{-7} s due to the large difference in temperature and heat capacity of the substrate and the single spray particles.

These thermal process conditions induce residual stresses in thermal spray coatings, which are mainly first due to this rapid solidification of the impinging particles and their shrinkage (which is restrained by the substrate), secondly due to different thermal expansions of the coating and the substrate caused by temperature gradients and the mismatch of the mechanical and thermophysical properties between coating and substrate (E, μ, α, λ, c_p), and thirdly due to the presence of non-uniform elastic or elastic–plastic deformations in the substrate and coating materials because of thermal and/or mechanical loading during heat and mass transfer in the coating deposition process (e.g., kinetic impact of semi molten or unmolten particles can induce compressive stresses). The first two residual stress mechanisms (quenching stress during particle deposition and thermal stress during temperature change of the component as a whole – both are transient stresses during the process and become residual stresses in the post-process steady state) are given schematically in Fig. 2 [25, 26].

Further contributions to the final state of residual stresses come from substrate pre-processing (e.g., machining or surface roughening and activation by grit blasting) and component post-processing to achieve the final surface quality needed (honing, polishing etc.). Grit-blasting and machining processes generally induce compressive residual stresses into the surface of substrate or coating, the extent and depth range depending on the blasting (time, distance, angle, velocity, and shot material used) or machining conditions and the materials properties [27]. An overview of the factors contributing to residual stresses is shown in Fig. 3.

The final residual stress state of a TS coating and the interface-near region in the substrate exert a major influence on its properties (bond strength, relaxation microcracks, wear mechanisms in tribology etc.) and reliability in application. Therefore, residual stress analysis is vital in layer composite characterisation and process optimisation. An overview about existing residual stress analysis methods, and especially these which are commonly used for thermal spray coating analysis, with a focus on the incremental, high-speed hole drilling/milling technique, are given in [1].

Experimental Setup and Measuring Procedure

The experimental setup for residual stress analysis (Fig. 4) can be divided into two parts: one for the machining of the object (see details in Laser machining system Section) and the other for the measurement of the resulting 3D displacements (see Measurement of the 3D displacements by digital holography section). An infrared pulsed laser (wavelength 1064 nm) and a cw laser (wavelength 532 nm) are used for the machining and the displacement measurements, respectively. The harmonic separator (HS in Fig. 4), transmits the infrared light and

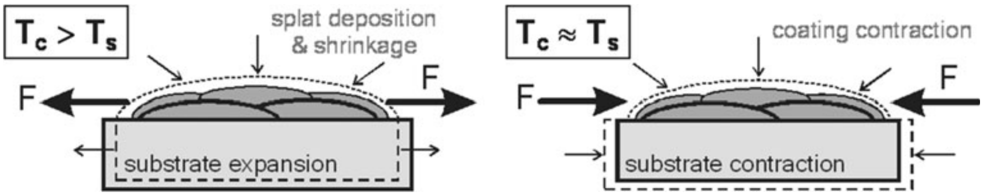

Fig. 2 Formation of quenching stresses during solidification of the coating (*left*) and thermal stresses during temperature change of the component (*right*, during the cooling period as an example) [24]

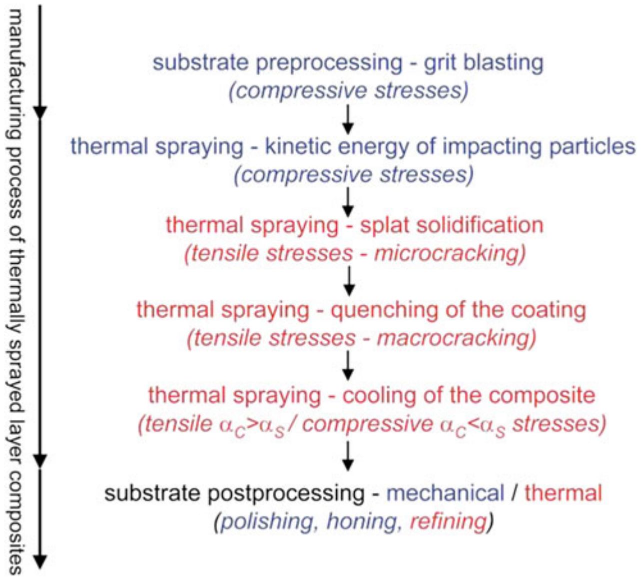

Fig. 3 Individual stress mechanisms during thermal spraying [28]

reflects the visible green light, allowing at the same time machining and displacement measurement.

Laser Machining System

Laser pulses with a power density higher than 10^9 W/cm^2 can be used for the ablation of material. In order to obtain such density, the laser beams having pulse lengths of some nanoseconds are focussed by a lens on the sample surface (see Fig. 5(a)). The minimal size of the laser spot is limited by the diffraction and is $S_{spot} = \lambda f / D$, where D, f and λ are: the aperture diameter of the beam incident on the lens, the focal length of the lens, and the wavelength of the laser, respectively. If we consider a wavelength $\lambda = 1064$ nm, a lens focal length $f = 200$ mm and an aperture $D = 10$ mm, then the spot size will be about 20 µm.

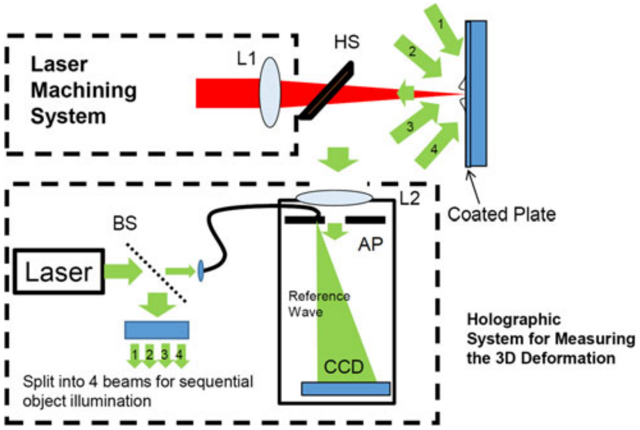

Fig. 4 Setup for laser machining and measurement of the 3D object displacement by digital holography. *HS* harmonic separator; *L1*, *L2* lenses; *BS* Beamsplitter; *AP* Aperture

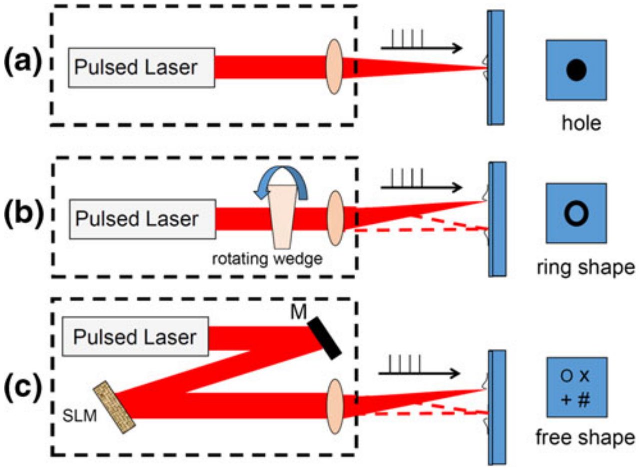

Fig. 5 Hole drilling by focussing the laser beam on the sample (**a**), ring shape milling by using a rotating wedge (**b**); free shape milling by using a SLM (**c**)

The laser spot on the surface may be easily increased by moving the object away from the focal point and this allows the drilling of larger holes if enough power density (>10^9 W/cm^2) is available.

A rotating wedge (see Fig. 5(b)) allows to direct the beam at different locations of the sample producing ring shape patterns. More complex structures can be machined by using two wedges; in this case the rotation of the wedges should be synchronised in order to produce the wanted pattern [21, 22]. It is also possible to use acousto-optical modulators (AOM) to direct the beam [29].

Spatial light modulators (SLM) have attracted lots of attention in various application areas due to their high spatial resolution and their direct programmability. A given light distribution may be produced by writing a phase/amplitude pattern (computer generated hologram) on the SLM (see Fig. 5(c)), and when the power density is large enough, this would enable laser machining [30]. The only disadvantage compared with the drilling/milling systems shown in Fig. 5(a–b) is that the SLMs are delicate and may be damaged by very high laser powers. The SLMs are available in transmission and reflection mode, some of them are based on a microelectromechanical system (MEMS), with several (e.g. 1000 × 1000) microscopic mirrors arranged in a rectangular array. The mirrors can be individually rotated to an on- or off-state and in this way modulate the amplitude. SLMs based on liquid crystals (LCD) allow phase modulation and have better efficiency compared with MEMS. Liquid-crystal-on-silicon (LCOS) are reflective modulators having over 90 % reflectance and a high fill factor. In our experiment, we used an LCOS from Holoeye (LC-R 3000) with 1920 × 1200 pixels in a display size of 18.2 × 11.4 mm^2, single pixel size of 9.5 µm.

Measurement of the 3D Displacements by Digital Holography

The release of residual stresses by the laser machining system produces 3D surface displacements that can be as small as 10 nm for the coating investigated in this work. These displacements can be measured by the system based on digital holography shown in the bottom part of Fig. 4. Light from a laser is divided into two beams by the beam splitter BS: one is coupled into a single mode optical fibre and serves as the reference beam and the other one is further divided into four beams illuminating the object sequentially from four different directions. The sequential illumination is done by using a computer controlled shutter (rotating disk with a hole) allowing to select which beam illuminates the object. Figure 6 shows a more detailed sketch of the object illumination geometry: $\vec{k}_1, \vec{k}_2, \vec{k}_3, \vec{k}_4$ are unit vectors pointing along the four illumination directions and $\vec{k}_0$ is a unit vector pointing in the observation direction. The light scattered by the object is reflected towards the holographic system by the harmonic separator (HS) and interferes with the reference forming a digital image plane hologram (since we use the lens L2 for imaging the surface of the object) which is recorded by the CCD. The phase of the wavefront is obtained by processing the digital hologram. In particular, a Fourier Transform of the recorded interference pattern is calculated (for this purpose, we use a FFT algorithm). In the Fourier plane a filter is applied in order to keep only the spatial frequencies corresponding to the wavefield. After an inverse Fourier transform, the amplitude and phase of the object wavefield is obtained [16].

The phase of the wavefront scattered by the object changes is a function of the displacement [15, 16]. When the object is illuminated along the directions $\vec{k}_i (i = 1, 2, 3, 4)$, the relations between the displacement vector $\vec{d}$ and the change of the optical phase $\Delta\phi_i$ is:

$$\Delta\phi_i = \frac{2\pi}{\lambda}\vec{d}\left(\vec{k}_i - \vec{k}_0\right). \tag{1}$$

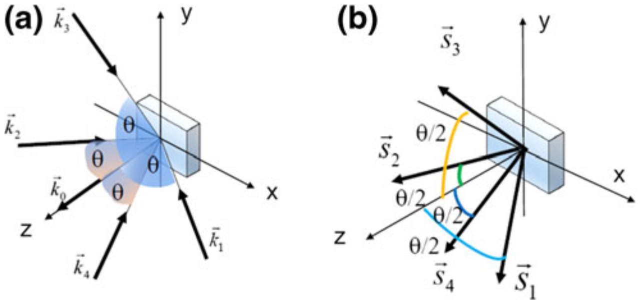

Fig. 6 Illumination of the object along the directions $\vec{k}_1, \vec{k}_2, \vec{k}_3, \vec{k}_4$; $\vec{k}_0$ is a unit vector pointing in the observation directions (**a**). Sensitivity vectors $\vec{s}_i = \vec{k}_i - \vec{k}_0$ (**b**)

As mentioned above, the holographic setup allows the detection of the phase, and thus, it is possible to detect the phase changes $\Delta\phi_i$ by processing holograms recorded before and after the displacement. According to equation (1), the components of the displacement vector $\vec{d} = \left(d_x, d_y, d_z\right)$ may be calculated when we have at least three independent phase differences $\Delta\phi_i$ (i = 1,2,3…). For our experiment, a symmetrical arrangement (see Fig. 6(a) with four illuminations parallel to the planes (x, z) and (y, z) was used; θ is the angle between the illuminations and the observation directions. For this arrangement, the sensitivity vectors $\vec{s}_i = \vec{k}_i - \vec{k}_0$ are (see Fig. 6(b)):

$$\begin{aligned} \vec{s}_1 &= \vec{k}_1 - \vec{k}_0 = (-\sin\theta, 0, 1 + \cos\theta) \\ \vec{s}_2 &= \vec{k}_2 - \vec{k}_0 = (\sin\theta, 0, 1 + \cos\theta) \\ \vec{s}_3 &= \vec{k}_3 - \vec{k}_0 = (0, -\sin\theta, 1 + \cos\theta) \\ \vec{s}_4 &= \vec{k}_4 - \vec{k}_0 = (0, \sin\theta, 1 + \cos\theta) \end{aligned} \tag{2}$$

The displacement vector $\vec{d} = \left(d_x, d_y, d_z\right)$ is calculated by a combination of the phase difference $\Delta\phi_i$ recorded by illuminating the object from the different directions and is given by:

$$d_x = \frac{\lambda(\Delta\phi_2 - \Delta\phi_1)}{4\pi\sin\theta} \tag{3.a}$$

$$d_y = \frac{\lambda(\Delta\phi_4 - \Delta\phi_3)}{4\pi\sin\theta} \tag{3.b}$$

$$d_z = \frac{\lambda(\Delta\phi_2 + \Delta\phi_1)}{4\pi(1 + \cos\theta)}. \tag{3.c}$$

In our experimental setup, we use a Nd:YAG laser (wavelength λ = 532 nm) and the holograms are recorded on a CCD camera (Vistek, ECO655) with 2448 × 2050 pixels, with an individual pixel size of $3.45 \times 3.45\ \mu m^2$. The angle θ, between the illumination directions and the z axis was chosen quite large (60°) in order to have a good sensitivity to in-plane displacements.

Measuring Procedure

The following procedure is applied for the measurements:

1. The object is illuminated sequentially from 4 directions and 4 holograms are recorded (it is possible to illuminate the object simultaneously from four directions and record the information about the 3D displacement in a single shot, but in this case, the quality of the measurements will be reduced due to the recording of four superimposed holograms in one frame [31])
2. A pulsed laser is used for machining the surface
3. The object is illuminated again from 4 directions and 4 holograms are again recorded

4. From the holograms recorded before and after the laser processing, the 3D displacement due to the surface machining (relaxation of residual stresses) are calculated.

The steps 2–4 are repeated M times, allowing the measuring of 3D displacements as a function of the incremental machining (thus, measuring residual surface strain/drilling depth profiles).

The phase difference $\Delta\phi_i$ in equation (1) is uniquely defined only in the range from −π to +π, and usually a phase unwrapping algorithm must be applied to obtain the real phase change. We avoided the phase unwrapping by loading the object in a way suitable to produce only small displacements, and thus, the corresponding phase changes $\Delta\phi_{i,n-1,n}$ between the machining done in steps $n-1$ and n are smaller than π. When this condition is satisfied, the phase change $\Delta\phi_{i,N}$ between the recording before the machining and the N machining steps is calculated by adding the phase changes measured between two successive steps:

$$\Delta\phi_{i,N} = \sum_{n=1}^{N} \Delta\phi_{i,n-1,n}. \tag{4}$$

Where the variable i can take the values 1,2,3,4 corresponding to the 4 illumination directions. The phase change due to the displacement produced by the first loading step is $\Delta\phi_{i,0,1}$. From the phase changes $\Delta\phi_{i,N}$, the 3D displacement vector between the state before the machining and machining step N can be determined according to equation (3). The addition procedure described by equation (4) may cumulate errors but since only few phases are added (typically 20–30), the errors cannot propagate too much. We did not use the "standard" approach by computing the phase difference with respect to the first recording followed by unwrapping since close to machined pattern the unwrapping is difficult due to the noisy phase produced by quite large displacements. If we consider only the displacements at a certain distance from the machined area then the standard approach may be used. By comparing the standard approach and the addition process described by equation (4) we did not notice significant differences (less than 5 nm when 16 phase differences are added).

It can be that from one machining step to the next the surface of the object will move with respect to the measuring system. These movements will produce unwanted linear phase changes in the recorded wavefront. Fortunately we know that the displacements due to laser loading are localized close to the machined area and thus the change of phase measured some mm from this area are due to unwanted rigid body movements that can be digitally compensated. Thus the phase differences in equation (4) need to be processed before addition in order to eliminate the unwanted phase changes.

At the begin of our investigations we were worried about the possible thermal effects due to the laser machining, in fact these could produce local deformations of the surface and influence the residual stress measurement. In one recent publication [32] we have shown that the temperature penetration depth is under 10 μm, hence, the corresponding thermal expansion may be neglected regarding its effect on surface displacement.

For the determination of the stresses, together with the 3D displacements, it is necessary to have the geometry of the machined surface (depth and shape of the hole) which can be obtained by direct measurement during the laser process, by calibration beforehand, or by simulation of the laser ablation process (which needs experimental verification, too). In our case, the second option was chosen, where the relation between the number of the fired pulses and the depth/shape of the hole was determined by measuring depth and shape of the hole (or other structured pattern) with white light or confocal microscopes after loading the surface with different sequences of laser pulses.

Figure 7 shows a diagram describing the development of the 3D surface displacement depending on the laser pulse sequence and the procedure used for the determination of the residual stresses at different depth of the coating by combination of: 3D displacements, shape/depth of the produced hole and material parameters.

Residual Stress Evaluation Procedure

As the mathematical background of residual stress determination shall not be the mayor part of this article, only some basics will be mentioned in the following. In principle, the removal of material which bears the residual stress $\vec{\sigma}$ will lead to a certain displacement $\vec{d}$ around the disturbed area. The correlation between hole geometry, coating and substrate material properties and the height of the displacement can be described by a calibration factor P of dimension [mm^3/N]. This leads to the equation

$$P\cdot\vec{\sigma} = \vec{d}. \tag{5}$$

If the removal is done in n sequential steps, $\vec{\sigma}$ and $\vec{d}$ are vectors with the size n. When an integral equation is used in order to determine the depth distribution for residual stresses, P has the size $n \times n$ with empty entries above its diagonal [33]. The integral method assumes the stress state in upper increments will influence the displacements when drilling deeper into the material. Therefore, a correlation between surface displacement and stress on every increment level must be found. This can be done by finite element method (FEM) simulations, where the exact hole geometry is modelled for every depth level and sequences of loads are, respectively, applied to every increment (Fig. 8).

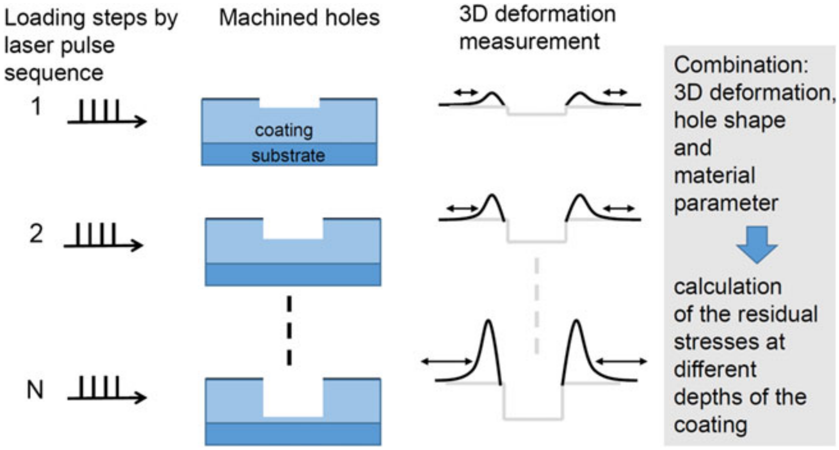

Fig. 7 Procedure for the determination of the residual stresses

While for conventional mechanical hole drilling measurements the strains are only determined with strain gauges, it is not convenient to evaluate the displacements from digital holography only on comparably localised areas. Rather all available data out of the displacement fields should be used in order to get more reliable results. Therefore, Schajer and Steinzig proposed in [10] to describe the correlation coefficients P_i as an integrated value around the hole with the inner radius r_i and the outer radius r_o for a cylindrical coordinate system

$$P_i = \frac{1}{r_o^2 - r_i^2} \int_{r_i}^{r^a} f(r)\ u(r)\ dr, \tag{6}$$

where u is the radial or axial displacement due to a hydrostatic load (index h), respectively the radial (index r), axial (index a) or circumferential (index Θ) displacement due to a deviator load (index d). This leads to a total of five necessarily known displacements, which have to be calculated by FEM. The function f is used for a weighting of the data in order to take rigid body movements of the specimen into account. In addition, the measured displacements can be written in an integral scheme

$$D_{c0} = \frac{1}{\pi\left(r_o^2 - r_i^2\right)} \int_{r_i}^{r^a}\int_{0}^{2\pi} f(r)\ d(r,\Theta)\ dr\ d\Theta, \tag{7}$$

$$D_{c1} = \frac{2}{\pi\left(r_o^2 - r_i^2\right)} \int_{r_i}^{r^a}\int_{0}^{2\pi} f(r)\ d(r,\Theta)\ \cos\Theta\ dr\ d\Theta \text{and} \tag{8}$$

$$D_{s1} = \frac{2}{\pi\left(r_o^2 - r_i^2\right)} \int_{r_i}^{r^a}\int_{0}^{2\pi} f(r)\ d(r,\Theta)\ \sin\Theta\ dr\ d\Theta, \tag{9}$$

where the indexes identify the trigonometric terms according to $\sin\Theta$, $\sin 2\Theta$, $\sin 3\Theta$ and equally for cosine terms [10]. Equation (5) can then be expressed as the following matrix operation (10), where $\vec{\sigma}$ is written as its hydrostatic (σ_h) and deviator (σ_d, σ_τ) parts. The resulting system of equations is over determined, hence, a least square method is used to find the solution. More details about the calculation and data processing can be found in [4, 5, 8, 10].

$$\begin{bmatrix} P_{h,z} & & \\ & P_{d,z} & \\ & & P_{d,z} \\ P_{h,r} & P_{d,r} & P_{d,\Theta} \\ P_{h,r} & P_{d,\Theta} & P_{d,r} \\ P_{h,r} & P_{d,\Theta} & P_{d,r} \\ P_{h,r} & P_{d,r} & P_{d,\Theta} \end{bmatrix} \begin{bmatrix} \sigma_h \\ \sigma_d \\ \sigma_\tau \end{bmatrix} = \begin{bmatrix} D_{c0} \\ D_{c2} \\ D_{s2} \\ D_{c1} + D_{c3} \\ D_{c1} - D_{c3} \\ D_{s1} + D_{s3} \\ D_{s1} - D_{s3} \end{bmatrix} \tag{10}$$

As mentioned above, it is crucial to use a proper hole geometry to calculate the correlation values P_i. Therefore, for conventional mechanical drillings an ideal cylinder is used. But the measurements of the surface after several laser ablation sequences showed a different geometry, more close to a frustum (Experimental results Section). The ablation rate per sequence and the structure of the ablated geometry were not constant, but for the FEM calibration a reliable geometry is required. For this reason, a program was developed to evaluate a best fit frustum approximation for the measured hole geometry after different number of pulses. Hence, white light interferometry measurements of the frustum were conducted after 50, 100, 200, 400 and 800 pulses. With that the progress of inner and outer hole radius and the hole depth can be found. Figure 9 shows the outer and inner radii are almost constant throughout the whole ablation process, with a mean radius of 372 µm. Only the first values scatter due to measurement errors for small hole depths. The depth in dependence of pulses can be described by a logarithmic regression.

Knowing these relations, it is possible to evaluate the hole geometry for every laser pulse, but the accuracy for depth <−100 µm is considerably low. Therefore, FEM

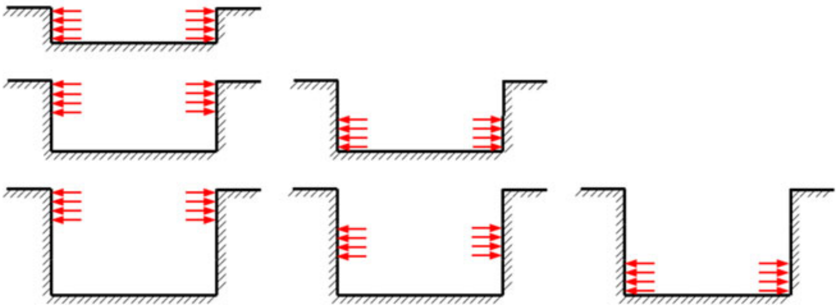

Fig. 8 Load application scheme for the integral determination of residual stresses [33]

calibration data were calculated for depths from −120 to −200 μm with intervals of 20 μm (Fig. 10) with the commercial tool Abaqus 6,12. Overall more than 10,000 C3D20 elements were used, while the area around the hole was modelled finest and attached to an outer part by a tie bonding (see also mesh detail in Fig. 10). The far ends of the model were 12 mm away from the center and symmetric boundary conditions were used on the X-Z- and Y-Z-plane. The load was applied directly on top of the hole surface for the calibration and as a overall predefined stress field for validation purposes. With comparative studies it was found out, that the numerical results are independent of the mesh size, the tie bonding and the distance to the outer boundary. Furthermore, the coating (Al_2O_3, Young's modulus 166 GPa, Poisson's ratio 0.23) was modelled with an ideal bonding on top of the substrate (aluminium, Young's modulus 68 GPa, Poisson's ratio 0.34).

In principle, the calculation of residual stresses for other geometries, i.e. notches for better geometric accuracy, follows the same rules. But the calibration has to be done for the corresponding geometry and the evaluation of displacement fields must be adapted to non-cylindrical surroundings. Especially for notches, a scheme where only displacements perpendicular to the hole are evaluated seems promising [34]. This subject is still work in progress.

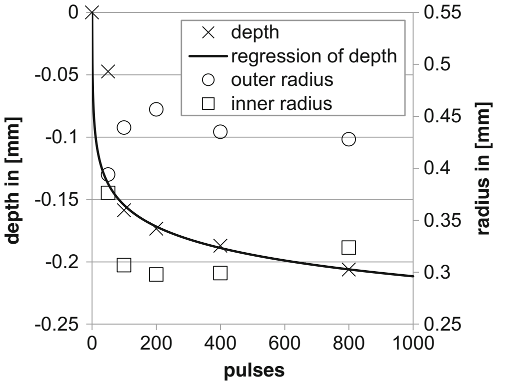

Fig. 9 Inner and outer radius and depth of the frustum as an approximation of ablated hole geometry; logarithmic regression of depth per pulse

Test Objects and Loading Device

Sample Preparation: Coating Deposition with the APS Method

Sample plates were prepared by grit blasting (surface roughening and activation), cleaning and coating application by atmospheric plasma spraying. The coating material was a mixed alumina/titania (Al_2O_3/ZrO_2 97/3) ceramic powder with grain sizes in the range of 5 up to 22 μm. The substrate plates were from aluminium (alloy 5754-H111), with sizes of $100 \times 100 \times 5$ mm^3 (referred to as plate A and B) and $100 \times 30 \times 5$ mm^3 (referred to as plate C).

The F6 plasma torch (GTV mbH, Luckenbach, Germany) was guided by a 6-axis robot for coating application. The spray process parameters that were constant for all coating processes are listed in Table 1. The spray path was a meander, and 6 (plate A) or 3 (plates B and C) coating passes were applied. Due to different numbers of passes as well as different substrate temperatures and process cooling techniques, the final coating thicknesses were different for each sample: 200 μm (plate A), 70 μm (plate B), and 180 μm (plate C). The coating thickness of the plates was measured by a Dualscope FMP100 with FTA probe (Helmut Fischer GmbH, Sindelfingen, Germany), based on eddy-current influence on a magnetic field.

Thermal process management was varied in order to take influence on the final residual stress situation: plates A and B were coated with the substrate preheated to 250 °C and without cooling during the process; plate C was not preheated, instead, simultaneous cooling by compressed air (front and back side of the plate) was applied to control temperature on a lower level. Thus, the peak temperature reached at the end of the deposition process in the coating (measured by IR pyrometry) was 500 °C (plates A and B) in comparison with 150 °C (plate C). Sample plate C was sprayed at such a low temperature in the attempt to deposit an almost residual stress free coating, which could then ideally be used to introduce load stresses at a well-defined stress level for validation of stress measurement results.

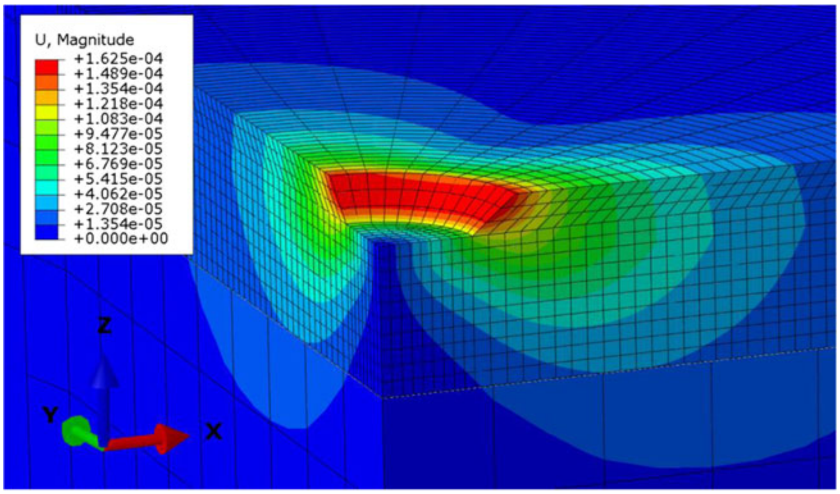

Fig. 10 Detail of the FEM model with coating (200 μm) and substrate for calibration of hole geometry; hole depth 120 μm, outer radius 440 μm; pure shear residual stress (100 MPa)

Comparative Residual Stress Analysis with the Hole Drilling Method

Determinations of the residual stresses in the sample plates were at first performed by the hole drilling method, based on mechanical machining (milling) of a hole of 1.8 mm diameter in incremental steps of 10 μm with a high-speed turbine and measurement of the resulting, 2-dimensional surface strains by means of 3-grid strain gauge rosettes with a diameter of 5.13 mm (standard strain gauges from Vishay Measurements) [1, 33, 35]. Figure 11 shows the measured strains (a, c, e) and the resulting residual stresses (b, d, f) for plates A, B, and C, as described above. The strains were measured along 3 directions 0, 45 and 90°, but because the results are very similar, only the 0° results are given in the figure. Residual stress calculation was performed by means of the differential method [1, 28, 36], and results are given in Fig. 11 in terms of principal residual stresses (as a function of drilling depth) for the same 0° orientation.

For plate A (Fig. 11(b)), the profile of the principal residual stresses presents a maximal value of −555 MPa at a depth of 230 μm. For plate B (see Fig. 11(d)), the profile of the principal residual stresses presents a maximal value of −245 MPa at a depth of 60–70 μm. The maximal values correspond well with the coating thickness in both cases (see coating thickness values above). Plate C shows only low residual stresses (see Fig. 11(f); maximal value of −70 MPa at 300 μm depth).

Table 1 APS coating process parameters

APS parameters		
Current	[A]	550
Gas flow rate (Ar/H_2)	[slpm]	55/12
Spray distance	[mm]	95
Pass distance	[mm]	3
Torch velocity	[mm/s]	350
Carrier gas flow rate (Ar)	[slpm]	12
Powder feed rate	[rev/min]	1.5

Experimental Results

In this section we will show some experimental measurements of 3D displacements produced by residual stresses relaxation with laser machined cut-outs using the systems shown in Fig. 5(a, c). Machining tests were carried out as well by the system using a rotating wedge (Fig. 5(b)) but in this case, the quality of the machining was not good due to the problem of synchronisation between the pulse firing and the wedge rotation. The results obtained with the machining method shown in Fig. 5(b) were not satisfying and are not shown.

Measurements of the Displacements Produced by Drilling a Hole with a Laser on a Coated Plate

The setup shown in (Fig. 5(a)) has been used to drill holes on the coating deposited on the plate A. The laser produces pulses with a duration of typically 10 ns and energy of up to 700 mJ with a repetition frequency of 20 pulses/second. Laser produced plasma plays an important role in the laser machining as it can partially block and absorb the incident laser beam [37]. It is thus convenient to adjust the energy of the laser in order to be just above the threshold necessary for the machining process. For our application we choose a pulse energy of 40 mJ. The lens used to focus the laser beam on the object surface has a focal length of 200 mm, the distance between the object and the laser focal point was adjusted (about 20 mm) in order to produce a laser spot diameter of 600 μm on the object surface, thus the power density (pulse energy/pulse duration/spot area) is $0.04\ \mathrm{J}/([10^{-8}\mathrm{s}]\times[\pi\ 0.03^2\ \mathrm{cm}^2]) = 1.4\times10^9\ \mathrm{W/cm}^2$, which allows the removal of the material. We found out that for each pulse, less than 1 μm material was removed, and therefore, to increase the removal, 25 pulses each having an

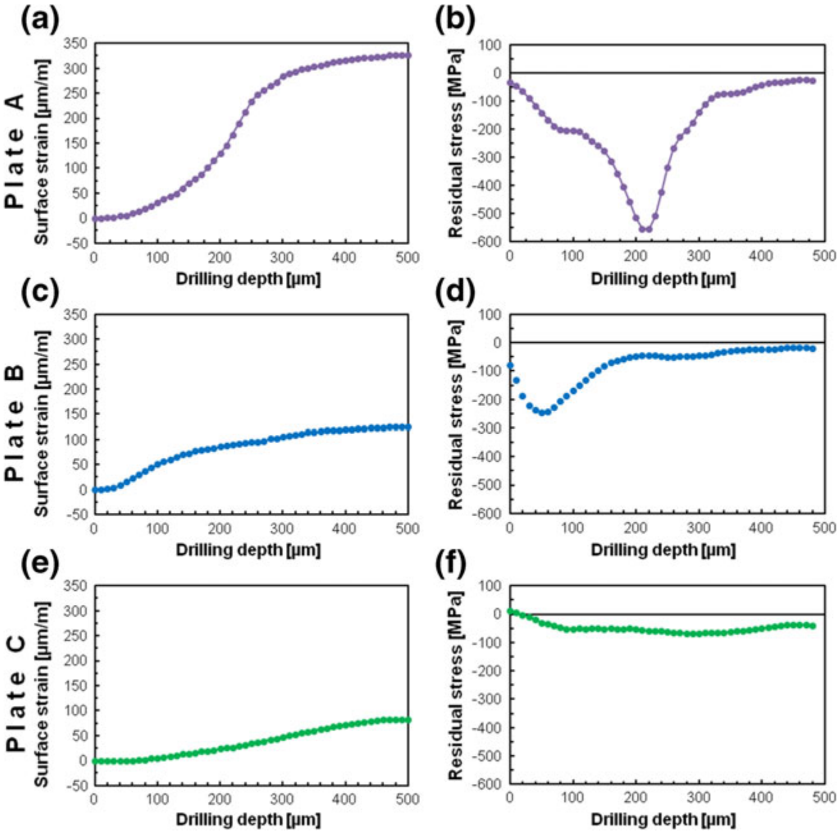

Fig. 11 Strain gauge rosette measurements during mechanical hole drilling experiments. Measured strain signals (**a**, **c**, **e**) and calculated principal residual stresses (**b**, **d**, **f**) for the three coated plates A, B, and C

energy of 40 mJ where fired for each machining step. After each machining step, the displacement of the object surface was measured. Figure 12(a, b) show the profiles of the hole after applying 2 × 25 pulses (2 machining steps) and 16 × 25 pulses (16 machining steps). Notice that the depth of the hole is not proportional to the applied number of pulses (see also Fig. 9), after 2 machining steps this was already 50 µm and after 16 the hole has a depth of approximately 200 µm (coating thickness). The reason for this nonlinear behavior is under investigation. The shape of the hole is approximately conical but not perfectly symmetrical due to the not homogeneous laser beam. Notice that by using the above mentioned power density, it was possible to drill the coating but not the aluminum substrate. Thus, even by applying more pulses the depth of the hole did not increase.

The distance between the object surface and the lens L2 (focal length 60 mm) of the measuring system (see Fig. 4) was 120 mm and the measurement of the displacements was done in a field of 7 × 7 mm^2. The phase modulo 2π (wrapped phases) corresponding to the displacements in the x, y (in-plane) and z (out-of plane) directions after 2 machining steps are shown in Fig. 12(c, d, e) and the displacements in Fig. 12(f, g, h), respectively. Figure 12(i, j, k, l, m, n) show phases and displacements after 16 machining steps. In all figures, the central part, having a diameter of 2 mm, was cut out. This part is larger compared with the diameter of the hole which is only 600 µm. It was removed since close to the hole the phase measured by the holographic method was very noisy and no information of the displacement can be retrieved there. The low quality of the measurements close to the hole is due to the change of the surface structure because of the laser machining. In the images we may see that the displacements are not perfectly symmetrical (see e.g. the phase maps in Fig. 12(e, k)), which is due to the quality of the laser beam.

Figure 13 shows the direction of the displacement of the in plane components obtained by combining the results shown in Fig. 12(l, m). The displacement is directed towards the centre (hole) and thus compressive stresses (negative) are inside the coating as expected from the measurements carried out by the strain gauge rosettes (see Fig. 8(b)). The measuring system allows the determination of the 3D displacement after each loading step. In Fig. 14, the x- displacements along a horizontal line for the loading steps 1 to 16 are shown, and the displacements increases with the number of applied loadings, but this increase is not linear. More loadings were applied, but after approximately 20 machining steps no further displacement was achieved, since as mentioned above the depth of the hole does not increase when the substrate is reached.

By knowing the shape of the hole and the displacement and using FEM models it was possible to determine the residual stresses [10] as a function of the depth by using the evaluation procedure described in "Residual stress evaluation procedure"

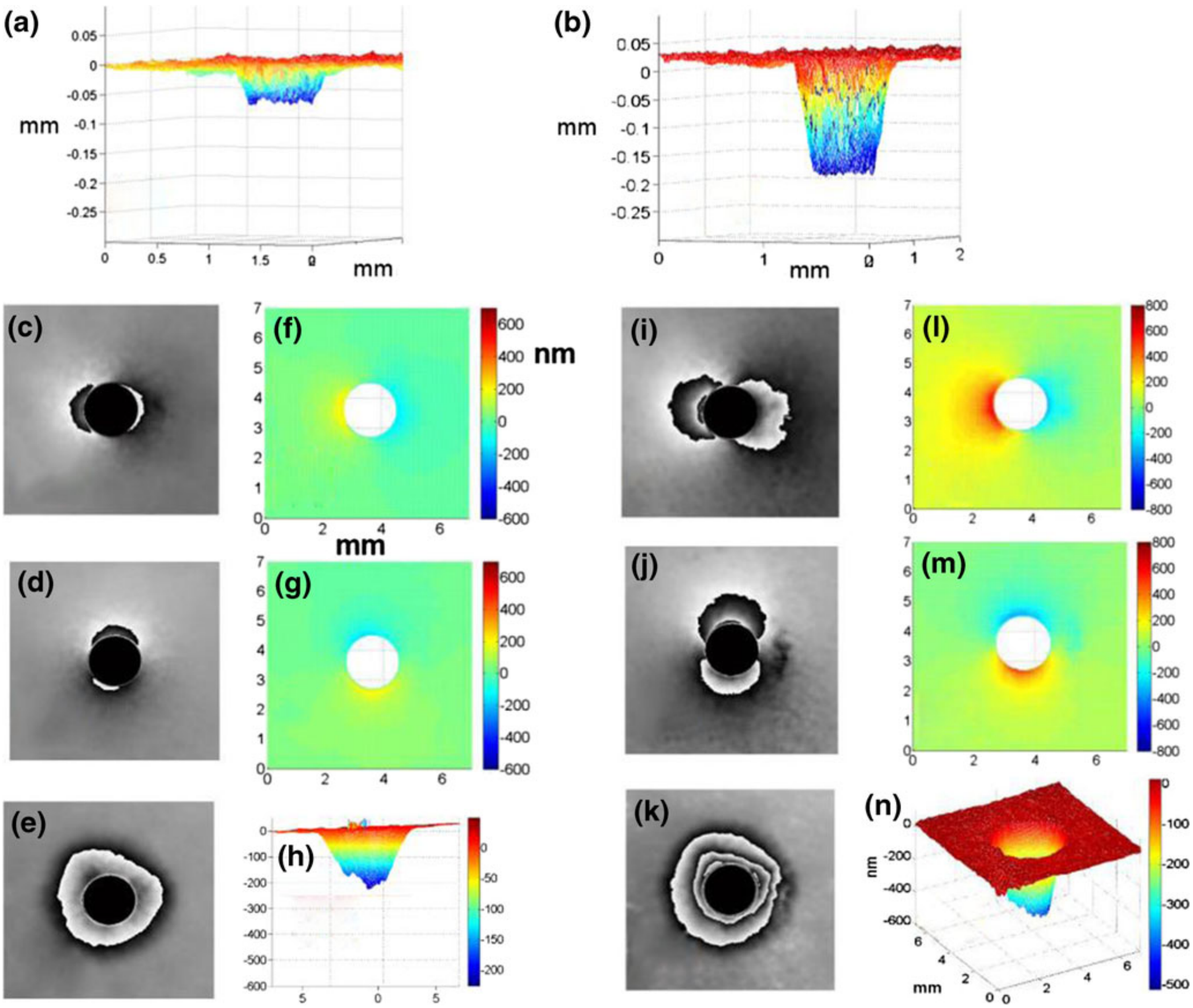

Fig. 12 Hole profiles after 2 (**a**) and 16 (**b**) machining steps. Phase modulo 2π (wrapped phases) and calculated displacements along the x (**c**, **f**), y (**d**, **g**) and z (**e**, **h**) directions after 2 machining steps. Phase modulo 2π and calculated displacements x (**i**, **l**), y (**j**, **m**) and z (**k**, **n**) after 16 machining steps

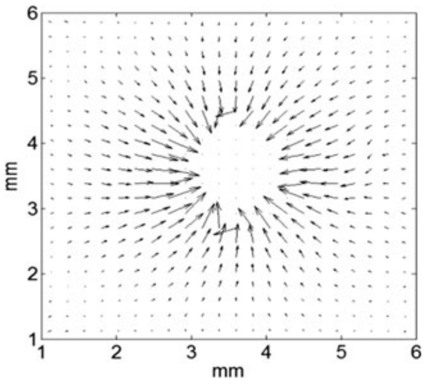

Fig. 13 Direction of the in plane displacements produced by the laser drilling

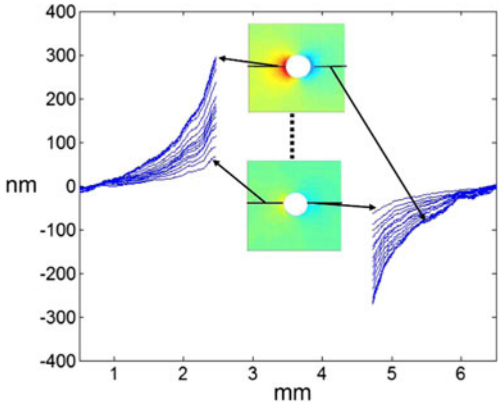

Fig. 14 Displacements along a horizontal line for different machining steps. The minimal load is for one machining step (25 pulses) and the maximal for 16 machining steps (16 × 25 pulses)

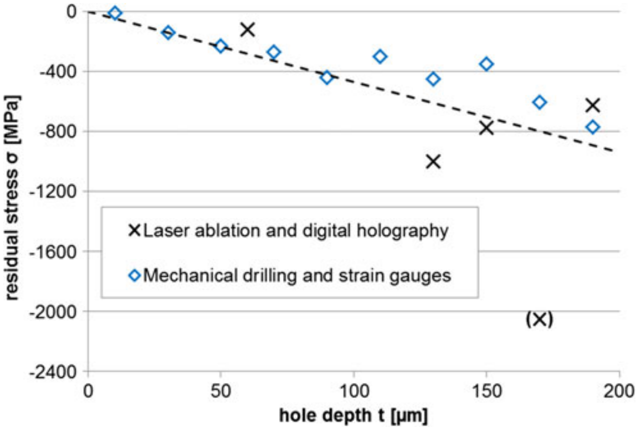

Fig. 15 Residual stress determined by conventional mechanical drilling and strain gauge measurement and the new proposed method with laser ablation and digital holography

Section. Figure 15 shown the results of the residual stress calculations by using conventional mechanical hole drilling with strain gauges and the proposed method with laser ablation and digital holography. The results have the same behaviour, we just have to point out that by using the holographic method the residual stresses were measured only at 5 depths (five crosses in the figure). While the stress value at a depth of 160 µm was considered as an outlier (deviation >5*medium deviation), a further rigorous error analysis of the accuracy of the results will be presented in another paper. Until now we may just say that the results obtained by the conventional hole drilling and the proposed methods show the same qualitative behaviour. The main reason for the occurring errors might be related to the inaccuracies due to the non-ideal geometry produced by laser ablation.

Measurement of 3D Displacements Produced by Free Form Laser Machining Using a SLM

The SLM based system shown in Fig. 5(c) was used for machining structures of arbitrary shape on the coated surface. One obvious example for residual stress relaxation and measurement purposes may be the milling of a linear notch, thus obtaining relaxation strains for the residual stresses being perpendicular to the notch. The SLM could be easily programmed to produce a bar shaped light distribution, but the pulse energy necessary to remove the material on the whole bar simultaneously would be high and this could damage the SLM. For this reason, another approach was chosen in which for each pulse, a spot of small size is focused on the surface, with the SLM modulating the position of the spot after each laser pulse. In this way, a bar shaped pattern may be produced by laser ablation. In our experiment, 200 pulses were used for milling the bar. If we apply the milling procedure one time, a bar having a depth of only few micrometers will be machined, but the depth of the structure is increased by repeating the procedure.

In this experiment, sample plate A was used (with 200 µm coating thickness; see in Fig. (8a, b) the results obtained by the hole drilling technique). Figure 16(a) shows the image of a 1 mm long milled horizontal bar obtained after 32 loading steps (1 loading step contains 200 pulses). In Fig. 16(b), the depth of the pattern after 1, 2, 4, 8, 16, and 32 steps is illustrated. These were measured by a white light interferometer and are 5, 10, 20, 40, 70, and 120 µm, respectively.

We applied 32 loading steps and measured the produced displacement after each step. Figure 16(c–h) show the wrapped phase and the corresponding 3D displacements produced by milling of the bar with 32 loading steps. Figure 17(a, b, c) show the x, y (in plane) and z (out-of-plane) displacements along a vertical (perpendicular to the notch) line for the loading steps 1 to 16. We may see that there is almost no displacement along the x direction (Fig. 17(a)) but the displacements are larger along y and z (Fig. 17(b, c)). In Fig. 17(b) we may notice as well that the first loading steps produce the strongest displacement. The results for steps 17 to 32 are not reported since almost no further displacement occurred. The direction of the in-plane displacements (Fig. 17(d)) shows that compressive stresses are inside the plate.

As already pointed out, this paper shall deal mainly with experimental details. Hence, within this paragraph only an overview over the used methods for determining the residual stress out of laser ablated notches is given. In principal the determination was done by applying an integral evaluation scheme on a rectangular approximation of the ablated notch. Therefore, the measured geometry of the ablated structure was transferred into a FEM mesh to get depth-dependent calibration coefficients (comparable to the hole evaluation in chapter 4). The depth increment size was 5 µm with a maximum depth of 200 µm. Compared to the hole geometry, the notch had an almost constant depth per sequence. Hence, out of the calibration it was able to use a bivariate interpolation to get exact coefficients for the ablated structures. But as the displacement field around a notch is no longer axial-symmetrical, a new approach was implemented, where only the displacements perpendicular to the notch were evaluated. The other displacements are considerably small. Furthermore, an area around the notch (a rectangle with a size of approximately 5×2.5 mm^2, with its long sides perpendicular to the ablated notch) is defined. Within this area the main deformations take place, why the calibration is calculated accordingly.

Figure 18 shows the results of the residual stress calculations by using conventional mechanical incremental hole drilling (IHD) with strain gauges and the proposed method with laser notch ablation and digital holography. The results obtained by the conventional hole drilling and the proposed methods show the same qualitative behaviour but of course there are

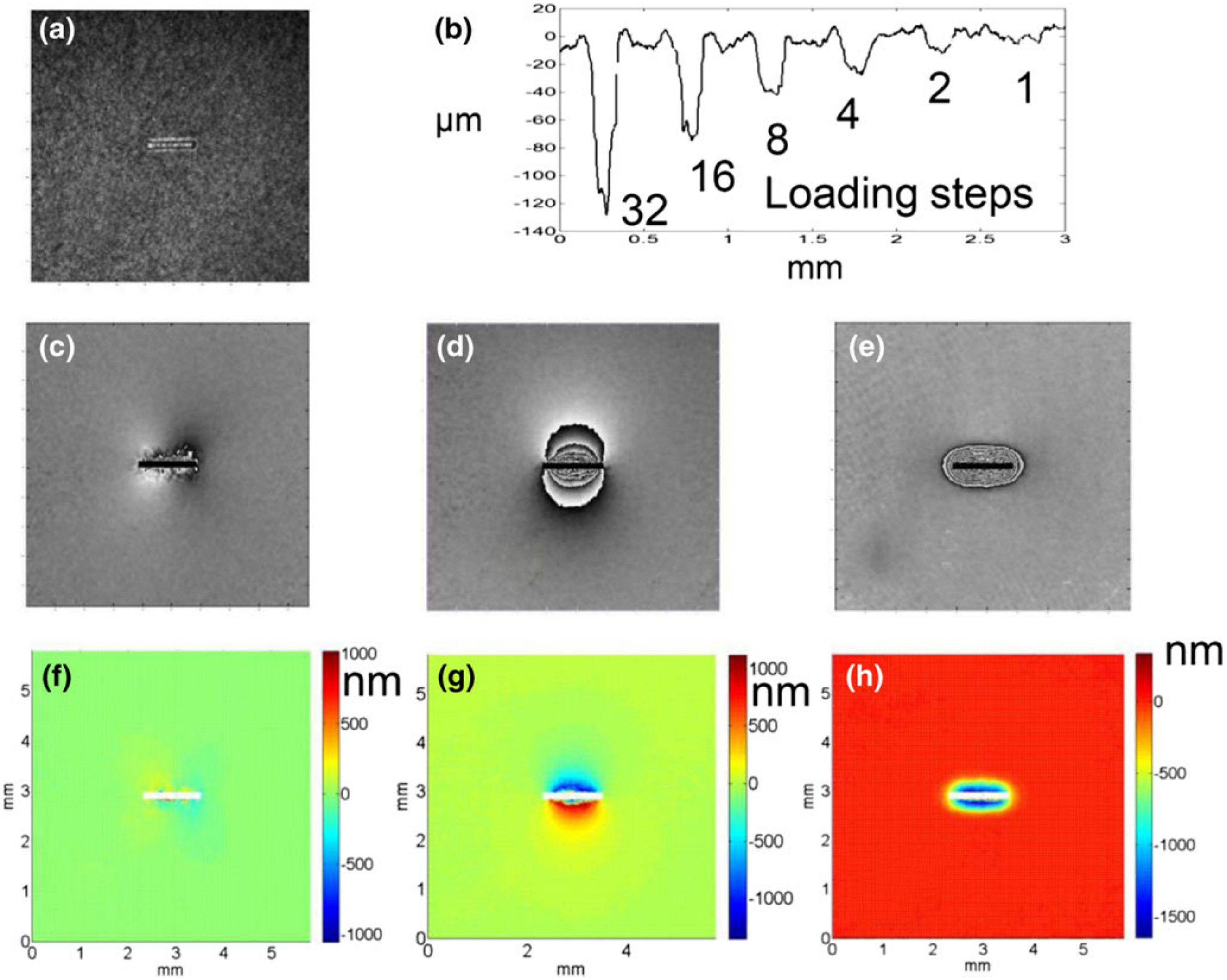

Fig. 16 Image of the bar shaped machined structure after 32 steps of loading (**a**). The depth profiles after 1, 2, 4, 8, 16, 32 loading steps (**b**). Phase modulo 2π (wrapped phases) and calculated displacements along the x (**c**, **f**), y (**d**, **g**) and z (**e**, **h**) after 32 loading steps

differences between the two curves. As already pointed out for the result shown in Fig. 15, the inaccuracies due to the non-ideal geometry produced by laser ablation may produce errors in the calculation of the residual stresses. It would be helpful to improve the quality of the laser milling in order to produce high accuracy pattern profiles. The measurement of the machined pattern (notch or other geometry) after each loading could be necessary in order to check if it has the expected shape and depth.

Figure 19 shows some results obtained by machining a notch in plate C. Figure 19(a, b, c) show three phase maps describing the displacements along the x (a), y (b) and z (c), respectively, for a machining process with 32 steps (each step has 200 pulses). The depth of the profile after 32 steps was 180 μm (thickness of the coating). By comparing these phase maps with those in Fig. 16(c, d, e), we may notice that the phases corresponding to the displacements in x and z directions are rather similar, but for the y direction (perpendicular to the horizontal bar) there are much less fringes and thus less displacement. This was expected since in this plate, there are less stresses, as shown in Fig. 11. Figure 19(d) shows the y-displacement along a vertical line obtained after the evaluation of the phase maps shown in Fig. 19(c). The maximal displacement in this case is about 80 nm and thus much less compared with the measurements shown in Fig. 17(b). Notice that the depth of the machined used for obtaining the results shown in Fig. 19 was 180 μm and thus larger compared with the 120 μm used for obtaining the results shown in Fig. 16 but the produced displacement much lower.

The SLM for modulating the pulsed laser beam was used for the milling of even more complex shaped structures on the thermal spray coating surfaces. The displacements produced by machining a cross shaped profile on the coating of Plate B, have been measured. For milling the cross, 200 pulses were used (100 for the 1 mm long horizontal bar and 100 for the 1 mm long vertical bar). The machined cross after 32 steps of

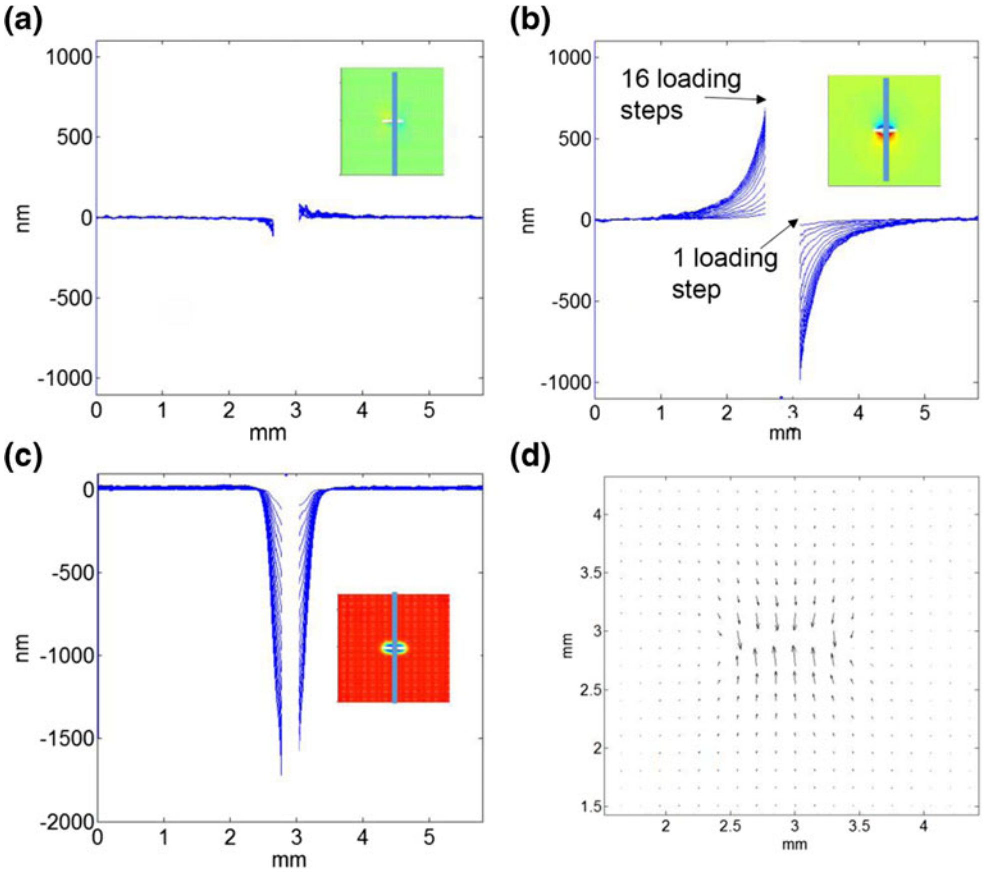

Fig. 17 Displacements in x (**a**), y (**b**) and z (**c**) measured along a vertical line for different loading steps. Direction of the in-plane displacements (**d**)

loading (32 × 200 pulses) and its magnified image are shown in Fig. 20(a, b), respectively. A white light interferometer was used to measure the machined cross profile, depths along vertical and horizontal lines are shown in Fig. 20(c, d). Notice that the horizontal bar is thicker, this is due to the fact that an elliptical spot (strongly elongated in the vertical direction) was used for machining. This ellipticity could be corrected and a cross having constant thickness could be easily machined. The wrapped phase and the corresponding 3D displacements produced by milling after 32 loading steps were calculated (Fig. 20(e–l)).

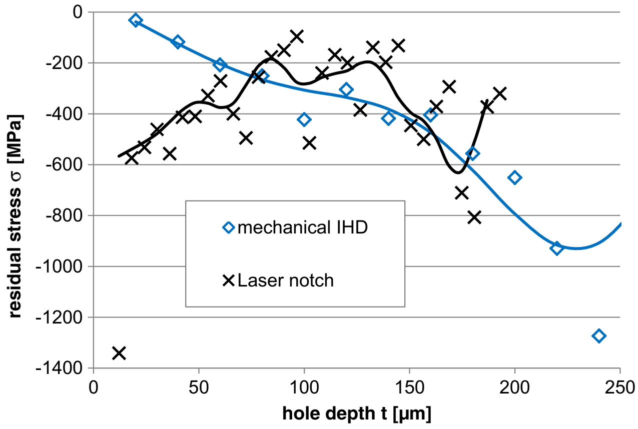

Fig. 18 Residual stress determined by conventional mechanical incremental hole drilling (IHD) and strain gauge measurement and the proposed method with laser notch ablation and digital holography

In another experiment, a ring shaped structure (diameter 1 mm) has been machined in the coating of plate B and the resulting 3D displacements have been measured. In Fig. 21(a), we see a micrograph of the ring structure obtained by applying 32 × 200 laser pulses. Due to elliptical laser spots (strongly elongated in the vertical direction), the width of the ring at the top and the bottom is thicker, and has different depth values compared to the middle (see Fig. 21(b, c)).

Figure 21(e–l) show the wrapped phases and the corresponding 3D displacements produced by milling a ring shape into the coating after 32 loading steps. In Fig. 21(m, n), the displacements along the two lines drawn in Fig. 21(h, i), are shown. From these profiles, we may see that the displacement along the x direction is larger compared with the displacement along the y direction. This behaviour is due to the asymmetrical machining of the ring. From the figures, we may see that it is possible as well to measure the displacement of the surface inside the machined ring. Since plate B contains compressive residual stresses, the surface outside the ring moves towards the center when the ring is machined. On the other side, the surface inside the ring moves in the opposite direction. This behavior can be clearly seen in the vectorial representation of the in-plane displacement (see Fig. 21(o)).

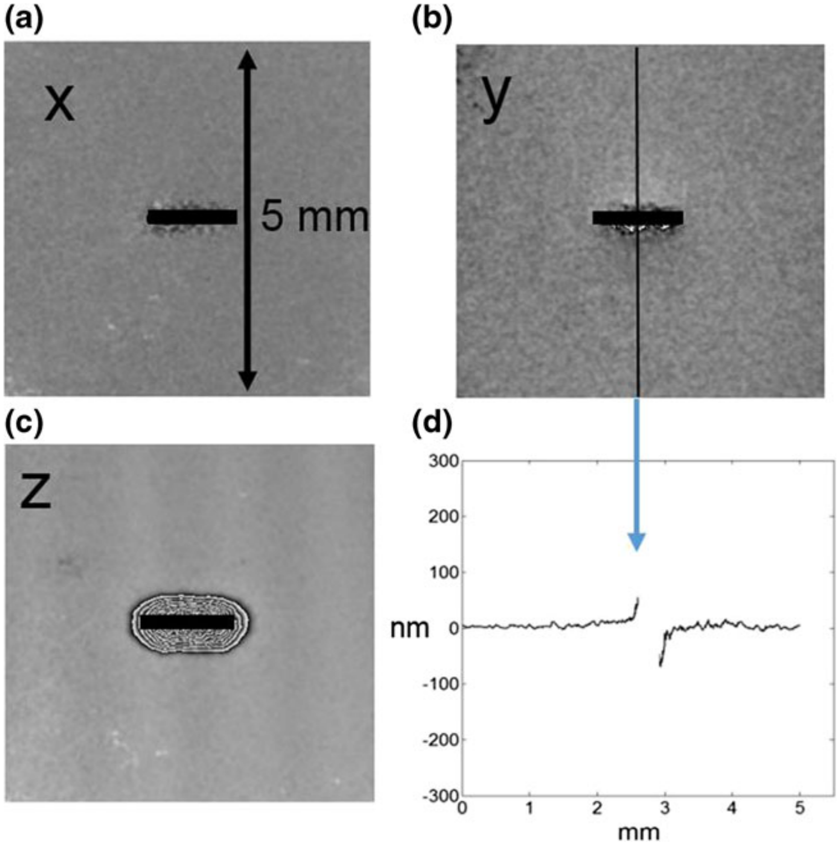

Fig. 19 Plate C. Phase modulo 2π (wrapped phases) corresponding to the displacements along x (**a**), z (**b**), y (**c**). Displacements along y (**d**)

A method for obtaining the residual stresses from the 3D-displacements produced by machining cross, ring or other structure is under investigation.

Errors in the Measurement of the Displacement and the Machined Profile

The accuracy of the measurement of the 3D displacement was determined by analyzing the noise for the case of no displacement of the sample (statistical analysis is used according to "The Guide to the Expression of Uncertainty in Measurement" GUM [38]; this is an incertitude of type A). The expected result should be 0, but due to the speckle noise, in-plane displacements of ±8 nm and out of plane displacements ±5 were measured. This represents the accuracy limit of the system. There are other sources of errors that may affect the accuracy of the measurement [39], in particular the accuracy in the determination of the angles of illumination and observation which are used to calculate displacements in Eq. 3. But these angles can be determined very accurately (±1°), and thus, the systematic error that they produce is negligible compared with the statistical error arising from the speckle noise.

For the measurement of the profile of the machined surface, we already use calibrated instruments. In particular, the white light interferometer and the confocal microscope used for the measurements had a vertical accuracy of 1 nm and lateral resolution of 0.5 μm. According to GUM [38], this is thus an uncertainty of type B.

Notice that this error analysis is restricted to the measurement of the machined profile and the measured 3D displacement. A rigorous analysis of the accuracy of the residual stresses calculated from the shape and displacement data will be the subject of another paper.

Conclusions

A system using a pulsed laser for machining of a surface and digital holography suitable for in-process measurement of the resulting 3D displacements that are due to relaxation of residual stresses in the material, was described. The obtained displacements together with the profile (shape, depth) of the surface machining pattern and the material parameters can be used to determine the residual stresses at different depths below the surface of a bulk material or a coating. The accuracy of the displacement measurement is ±8 nm, and thus, well suited to retrieve relaxation strains from which residual stresses can be obtained. For the particular case of drilling a hole with a laser, the residual stresses were calculated for coated sample materials and are in agreement with the results obtained by using the standard, mechanical hole drilling strain gauge method. Investigations that should allow the calculation of

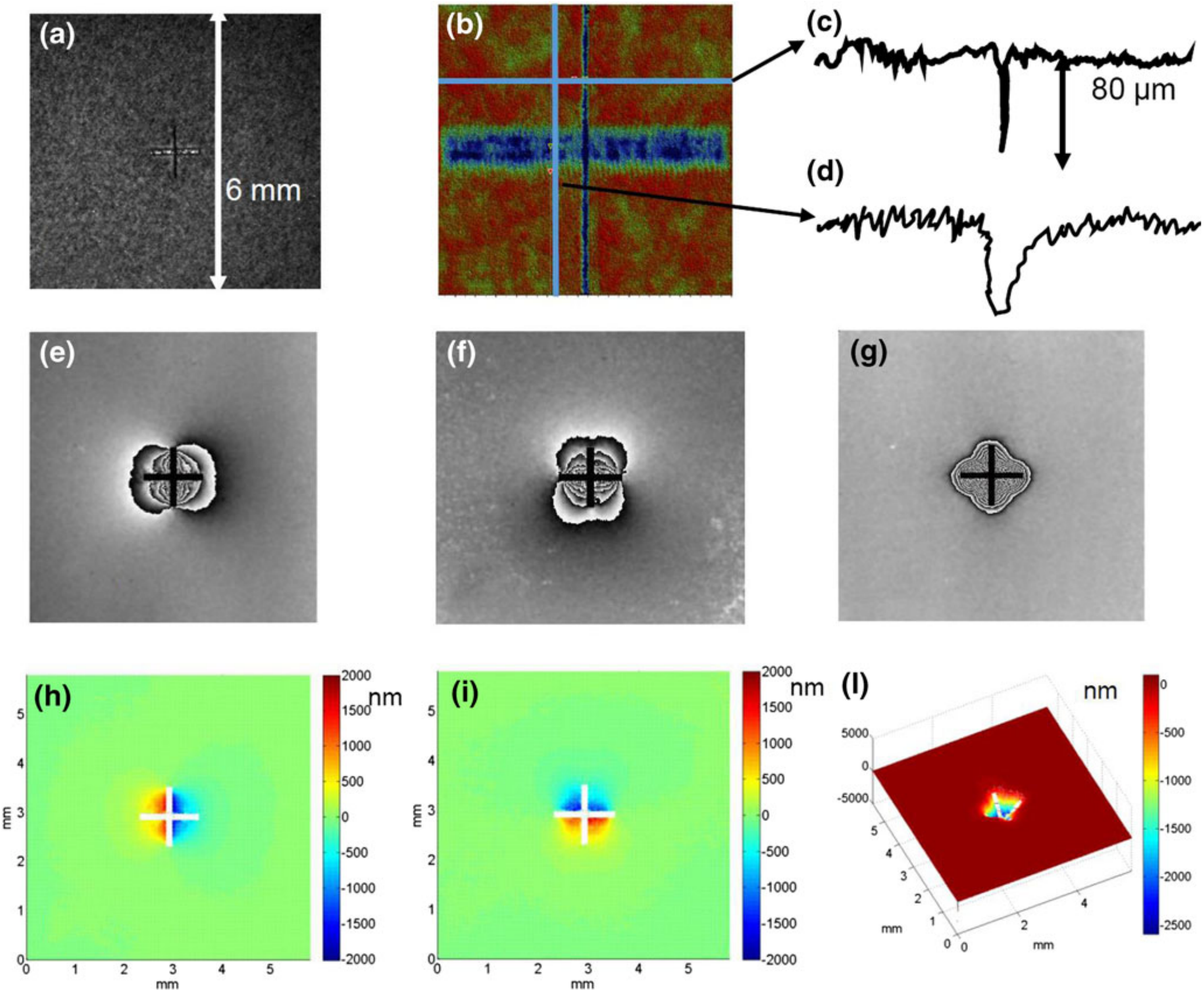

Fig. 20 Cross shaped structure machined with the SLM after 32 steps of loading (**a**). The depth profiles (**c**) and (**d**) along the lines shown in (**b**). Phase modulo 2π (wrapped phases) and calculated displacements along the x (**e**, **h**), y (**f**, **i**) and z (**g**, **l**) after 32 loading steps

residual stresses at different depths from the displacement produced by laser milling of complex shapes (bars, rings, crosses) are still in progress.

The test plates used for validation of the technique were aluminium substrates, on which alumina/titania (Al_2O_3/ZrO_2 97/3) coatings were deposited by the atmospheric plasma spraying technique. By control of the spray parameters, coatings with large compressive residual stresses as well as almost stress-free coatings were obtained.

Compared with the standard hole drilling technique, the method presented in this paper has the advantage that the machining is done without mechanical contact by using a pulsed laser. Furthermore, the use of a SLM modulator allows more flexibility in the machining, producing not only circular holes but also more complex structures of arbitrary shape. As a further advantage, measurement of the surface displacements is done optically and does not require the application of devices (such as strain gauges, which require a high degree of accuracy during application and which are not applicable on every surface) or manipulations on the surface (like polishing, lacquering or similar).

Due to the fact that machining and measurement are achieved without contact, the method permits (in principle) in-process measurement and can thus improve the hole drilling residual stress analysis, allowing not only for residual stress detection in static condition after component processing, but also the in-process measurement of process-induced, transient stresses (thermal stresses, coating solidification stresses etc.). The next step of our investigations will be to implement a system using laser machining as well as displacement and shape measurement during the coating application process. This would lead to an increased understanding of residual stress evolution, especially a weighting of the different contributing phenomena to the final state of residual

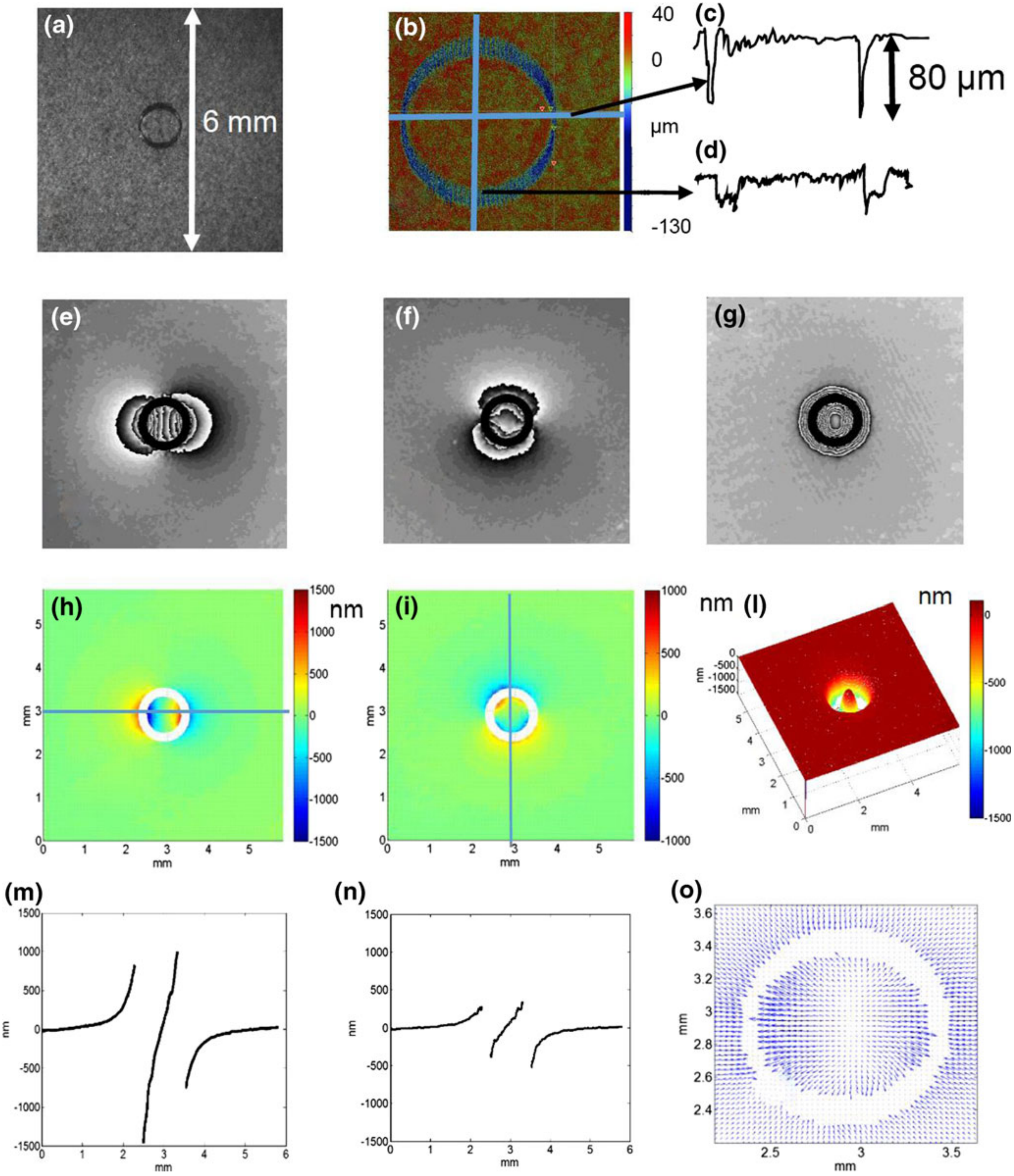

Fig. 21 Ring shaped structure machined with the SLM (**a**). The depth profiles (**c**) and (**d**) along the lines shown in (**b**). Phase modulo 2π (wrapped phases) and calculated displacements along the x (**e**, **h**), y (**f**, **i**) and z (**g**, **l**). Profile of the displacements along x (**m**) and y (**n**) taken on the horizontal and vertical lines in (**h**) and (**i**) Directions of the displacements (**o**)

stresses, and could enable the manufacturing of coated parts with a residual stress state that lies within narrow limits of application oriented, predefined residual stress specifications.

During the experiments described in this paper, the system for laser machining and 3D measuring were located on a laboratory table. Thus, it is expected that some problems will arise when it will be transferred in an industrial environment. In particular, the sample will vibrate with respect to the measuring system and produce additional straight fringes in the phase that need to be compensated, and the spray torch will frequently interfere with the line of sight of the system.

The method was developed for the machining and measurement of coated surfaces, but it could be used as well for other kind of applications where residual stresses inside an object (close to its surface) need to be determined, i.e. hard materials, where a mechanical drilling is not possible or small objects, on whom strain gauge rosettes cannot be placed.

Acknowledgments This work was supported by the German Research Foundation (DFG) under Grant nos. Schm746/120, GA589/10 and OS111/37.

References

1. Wenzelburger M, López D, Gadow R (2006) Methods and application of residual stress analysis on thermally sprayed coatings and layer composites. Surf Coat Technol 201(5):1995–2001
2. Heimann RB (1996) Plasma-spray coating: principles and applications. VCH Verlagsgesellschaft mbH. ISBN: 3-527-29430-9
3. Altpeter I, Becking R, Kern R, Kröning M, Hartmann S (1999) Mikromagnetische Ermittlung von thermisch induzierten Eigenspannungen in Stählen und weißem Gußeisen. In: von Aurich D, Kloos K-H, Lange G, Macherauch E (eds) Eigenspannungen und Verzug durch Wärmeeinwirkung. Wiley-VCH, Weinheim, pp 407–426, Forschungsbericht zum gleichnamigen Schwerpunkt-programm der DFG
4. Schajer GS, Prime MB (2006) Use of inverse solutions for residual stress measurements. J Eng Mater Technol 125(3):375–382
5. Schajer GS, Rickert TJ (2011) Incremental computation technique for residual stress calculations using the integral method. Exp Mech 51(7):1217–1222
6. Schajer GS, Abraham C (2014) Residual stress measurements in finite-thickness materials by hole-drilling. Exp Mech 54:1515–1522
7. Schajer GS, Whitehead PS (2013) Hole drilling and ring coring. In: Schajer GS (ed) Practical residual stress measurement methods, chapter 2. Wiley, Chichester
8. Steinzig M, Ponslet E (2003) Residual stress measurement using the hole drilling method and laser speckle interferometry. Exp Tech 27(3):43–46
9. Baldi A (2005) A new analytical approach for hole drilling residual stress analysis by full field method. J Eng Mater Technol 127:165–169
10. Schajer GS, Steinzig M (2005) Full-field calculation of hole-drilling residual stresses from ESPI data. Exp Mech 45(6):526–532
11. An Y, Schajer GS (2010) Pixel quality evaluation and correction procedures in ESPI. Exp Tech 105:106–112
12. Viotti M, Suterio R, Albertazzi A, Kaufmann G (2004) Residual stress measurement using a radial in-plane speckle interferometer and laser annealing: preliminary results. Opt Lasers Eng 42:71–84
13. Viotti M, Albertazzi A, Kapp WA (2008) Experimental comparison between a portable DSPI device with diffractive optical element and a hole drilling strain gauge combined system. Opt Lasers Eng 46: 835–841
14. Viotti M, Kapp W, Albertazzi A (2009) Achromatic digital speckle pattern interferometer with constant radial in-plane sensitivity by using a diffractive optical element. Appl Opt 48:2277–2281
15. Seebacher S, Osten W, Baumbach T, Jüptner W (2001) The determination of material parameters of microcomponents using digital holography. Opt Lasers Eng 36:103–126
16. Pedrini G, Osten W, Gusev ME (2006) High-speed digital holographic interferometry for vibration measurement. Appl Opt 45: 3456–3462
17. Sutton MA, Orteu JJ, Schreier HW (2009) Image correlation for shape, motion and deformation measurements: basic concepts, theory and applications. Springer, New York
18. Mix PE (2005) Introduction to nondestructive testing. A trainin guide, 2nd edn. Wiley, Hoboken
19. Baldi A (2014) Residual stress measurement using hole drilling and integrated digital image correlation techniques. Exp Mech 54:379–391
20. von Allmen M (1976) Laser drilling velocity in metals. J Appl Phys 47:5460
21. Dausinger F, Hugel H, Konov VI (2003) Micromachining with ultrashort laser pulses: from basic understanding to technical applications. Proc. SPIE 5147, ALT'02 International Conference on Advanced Laser Technologies 106. doi:10.1117/12.537496
22. Dhar S, Saini N, Purohit R (2006) A review on laser drilling and its Techniques. Proceedings: International Conference on Advances in Mechanical Engineering-2006 (AME 2006). Baba Banda Singh Bahadur Engineering College, Fatehgarh Sahib, Punjab, India
23. Standard DIN EN 657:2005–06: Thermal spraying – terminology, classification (German Version)
24. Buchmann M, Gadow R, Tabellion J (2000) Residual stress optimization of thermally sprayed ceramic coatings on light metal components. In: Gadow R (ed) Advanced Ceramics and Composites / 6th Interregional European Colloquium on Ceramics and Composites, expert, Renningen, p 268–281. ISBN 3-8169-1830-1
25. Elsing R, Knotek O, Balting U (1990) The influence of physical properties and spraying parameters on the creation of residual thermal stresses during the spraying process. Surf Coat Technol 41(2): 147–156
26. Kuroda S, Clyne TW (1991) The quenching stress in thermally sprayed coatings. Thin Solid Films 200(1):49–66
27. American Welding Society (ed) (1985) Thermal spraying: practice, theory, and application. American Welding Society AWS, Miami (FL), USA. ISBN 0-87171-246-6
28. Gadow R, Riegert-Escribano MJ, Buchmann M (2005) Residual stress analysis in thermally sprayed layer composites, using the hole milling and drilling method. J Therm Spray Technol 14(1):100–108
29. Venkatakrishnan K, Stanley P, Lim L (2002) Femtosecond laser ablation of thin films for the fabrication of binary photomasks. J Micromech Microeng 12:775
30. Beck RJ, Waddie AJ, Parry JP, Shephard JD, Taghizadeh MR, Hand DP (2011) Adaptive laser beam shaping for laser marking using spatial light modulator and modified iterative fourier transform algorithm. Phys Procedia 12:465–469
31. Schedin S, Pedrini G, Tiziani HJ, Mendoza Santoyo F (1999) Simultaneous three-dimensional dynamic deformation measurements with pulsed digital holography. Appl Opt 38:7056–7062
32. Weidmann P, Weber U, Schmauder S, Pedrini G, Osten W (2015) Numerical calculation of temperature and surface topology during a laser ablation process for ceramic coatings. Meccanica 1–11. doi: 10.1007/s11012-015-0220-2
33. ASTM E 837–13 (2013) Standard test method for determining residual stresses by the hole-drilling strain-gage method
34. Schajer GS (2010) Relaxation methods for measuring residual stresses: techniques and opportunities. Exp Mech 50:1117–1127
35. Mathar J (1933) Ermittlung von Eigenspannungen durch Messung von Bohrloch-Verformungen. Archiv fur das Eisenhuttenwesen 6(7):277–281

36. Häusler H, König G, Kockelmann H (1987) On the accuracy of determining the variation with depth of residual stresses by means of the hole-drilling method. In: Macherauch E, Hauk V (eds) Residual stresses in science and technology, vol. 1 (Int. Conf. On Residual Stresses, Garmisch-Partenkirchen, 1986), DGM Informationsgesellschaft, Oberursel, p 257–264
37. Varier GK, Issac RC, Harilal SS, Bindhu CV, Nampoori VPN, Vallabhan CPG (1997) Investigations on nanosecond laser produced plasma in air from the multi-component material $YBa_2Cu_30_7$. Spectrochim Acta B 52:657–666
38. International Standardization Organization (ISO) (1995) Guide to the expression of uncertainty in measurement (GUM), Geneva
39. Pedrini G, Gaspar J, Schmidt ME, Alekseenko I, Paul O, Osten W (2011) Measurement of nano/micro out-of-plane and in-plane displacements of micromechanical components by using digital holography and speckle interferometry. Opt Eng 50(10):101504